

基于双箭头超表面宽带太赫兹涡旋光束的产生

郭姣艳^{1,2,3}, 李文宇^{1,2,3}, 孙然^{1,2,3}, 赵国忠^{1,2,3*}¹首都师范大学物理系, 北京 100048;²北京成像理论与技术高精尖创新中心, 北京 100048;³首都师范大学太赫兹光电子学教育部重点实验室, 北京 100048

摘要 涡旋光束在提高通信能力方面的巨大潜力日益受到人们的青睐,而宽带特性是提高信道容量的关键。此外,当前涡旋光束产生器件存在着带宽窄、效率低等缺点。因此,设计了一种基于 Pancharatnam-Berry 相位的超宽带反射超表面,该超表面由 13×13 单层旋转反射单元结构组成,在频率范围为 $0.9 \sim 1.8$ THz 内可产生太赫兹涡旋光束。结果表明,该涡旋光束产生器件可以实现高效率(工作效率在 90% 以上)和较宽的工作频率,这为高性能宽带涡旋光束产生器的设计开辟了一条新途径。

关键词 光通信; 太赫兹; 涡旋光束; 宽带; 超表面

中图分类号 O436

文献标志码 A

doi: 10.3788/CJL202148.2014003

1 引言

太赫兹波是一种电磁波,介于微波与红外之间,具有一些其他波段所没有的特殊性质。随着太赫兹科学技术的发展,太赫兹技术在光谱^[1-2]、成像^[3-4]、无损检测^[5]、通信^[6]等领域中的应用越来越广泛。近年来,携带轨道角动量(OAM)的涡旋光束引起了研究人员的广泛关注^[7-8]。OAM 涡旋光束具有相位因子 $\exp(il\varphi)$, φ 是方位角, l 是拓扑荷(取值可以是整数或非整数)^[9]。涡旋光束的波前螺旋向前传播,且光束中心的强度接近于零^[10-11],这种独特的电磁特性在光学、原子物理和通信领域中有着潜在的应用^[12-13]。迄今为止,研究人员已经提出了很多产生涡旋光的方法,如螺旋相位板^[14]、空间光调制器(SLM)^[15-16]、衍射相全息图^[17]等。虽然利用上述方法设计的光学器件易于实现,但是这些器件存在着尺寸大、价格昂贵、信息不能长距离传输等问题。因此,基于超表面的涡旋光束产生受到了广大学者的关注。超表面可以对电磁波波前相位、振幅及偏振进行调控,是一种不同于传统材料的新颖结构材

料^[18]。基于超表面的涡旋相位板不仅结构简单,还能减小损耗,这有利于其集成化发展。

近些年,对涡旋光的研究越来越多,不仅涉及可见光和微波波段,还涉及太赫兹波段。2011年, Yu 等^[19]设计了 V 字型天线,利用 8 个相位间隔 45° 的 V 字型单元结构排布的超表面引入相位不连续性的方式,实现了红外波段相位 $0 \sim 2\pi$ 的分布,产生了涡旋光束。2013年, He 等^[20]提出了基于互补型 V 型单元结构的超表面,实现了在太赫兹波段产生涡旋光束。2016年, Yu 等^[21]设计了由不同臂长的交叉偶极子单元组成的超表面,证明了在单一频率下,利用反射式超表面可产生双极化双模的涡旋光束。2017年, Xu 等^[22]利用共极化模式产生了宽带涡旋光束,工作频段内的效率为 82%。虽然超表面产生涡旋光束的研究从单频点扩展到了宽频段上,但是存在工作效率不高的问题。因此,本文提出了一种基于 Pancharatnam-Berry (P-B) 相位的反射超表面,不仅提高了太赫兹涡旋光束的工作带宽(频率范围为 $0.9 \sim 1.8$ THz),工作效率还达到了 90% 以上。

收稿日期: 2021-01-07; 修回日期: 2021-01-11; 录用日期: 2021-03-29

基金项目: 国家自然科学基金(62071312)

通信作者: *guozhong-zhao@cnu.edu.cn

2 单元结构的分析与设计

2.1 理论分析

电磁波所携带的角动量可以分为自旋角动量 (SAM) 和 OAM, 分别与偏振和空间相位分布有关。SAM 只具有两个广义态 $\pm \hbar$, 代表着左右圆极化。OAM 具有 $l\hbar$ 个值, 其中 $\hbar = h/(2\pi)$, h 为普朗克常量, \hbar 为一个光子的自旋角动量。由于 OAM 的不同状态是相互正交的, 并且可以携带不同的信息, 因此具有 OAM 的涡旋光束在通信领域中有着广阔的应用前景^[23]。

为了产生宽带涡旋光, 设计了一个由单层双箭头金属结构单元组成的超表面。该单元结构可独立控制入射波和反射波, 且旋转单元结构可实现宽带特性和相位变化。

当一束平面波垂直照射到反射型超表面单元结构上时, 以单元结构传播方向为旋转轴, 绕其中心逆时针旋转 θ 角, 其反射矩阵^[24]可以表示为

$$\mathbf{R}_\theta^{XY} = \begin{bmatrix} \cos \theta & -\sin \theta \\ \sin \theta & \cos \theta \end{bmatrix}^{-1} \begin{bmatrix} r_{xx} & r_{xy} \\ r_{yx} & r_{yy} \end{bmatrix} \begin{bmatrix} \cos \theta & -\sin \theta \\ \sin \theta & \cos \theta \end{bmatrix}, \quad (1)$$

式中: $\begin{bmatrix} \cos \theta & -\sin \theta \\ \sin \theta & \cos \theta \end{bmatrix}$ 表示旋转矩阵;

$\begin{bmatrix} \cos \theta & -\sin \theta \\ \sin \theta & \cos \theta \end{bmatrix}^{-1}$ 表示旋转矩阵的逆矩阵;

$\begin{bmatrix} r_{xx} & r_{xy} \\ r_{yx} & r_{yy} \end{bmatrix}$ 表示反射传输矩阵, 其中 r_{xx} 表示当线偏振光沿 x 轴正方向入射时, 其沿 x 轴负方向出射的反射系数, 矩阵中的 r_{xy} 、 r_{yx} 、 r_{yy} 与 r_{xx} 的定义类似;

上标 XY 表示沿 Y 方向偏振的入射线偏振光, 出射后变成沿 X 方向偏振的线偏振光。图 1 为在笛卡儿坐标系下, 旋转 θ 角前后的单元结构, 其中 u 、 v 为旋转 θ 角后的坐标轴。

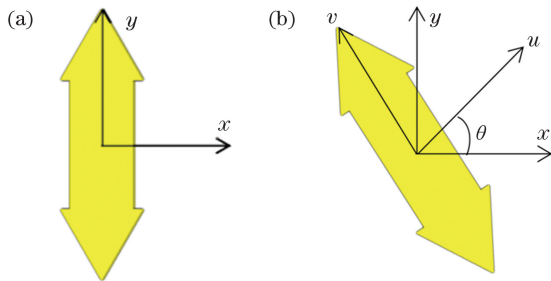


图 1 在笛卡儿坐标系下, 旋转 θ 角前后的单元结构

Fig. 1 Element structures before and after rotating θ angle in Cartesian coordinate system

为了将线偏振反射矩阵转换为圆偏振反射矩阵, 利用变换矩阵 $\frac{1}{\sqrt{2}} \begin{bmatrix} 1 & 1 \\ j & -j \end{bmatrix}$ 可以得到当圆偏振光入射到单元结构, 且单元结构绕其中心逆时针旋转 θ 角时的反射矩阵

$$\mathbf{R}_\theta^{LR} = \frac{1}{2} \begin{bmatrix} 1 & -j \\ 1 & j \end{bmatrix}^{-1} \mathbf{R}_\theta^{XY} \begin{bmatrix} 1 & -j \\ 1 & j \end{bmatrix}, \quad (2)$$

式中: L、R 分别表示入射光为左旋圆偏振波和右旋圆偏振波。

将(1)式代入(2)式中, 可推导出圆偏振波入射下的反射矩阵为 $\begin{bmatrix} r_{LL} & r_{LR} \\ r_{RL} & r_{RR} \end{bmatrix}$, 其中

$$\begin{cases} r_{LL} = \frac{1}{2} [(r_{xx} - r_{yy}) - j(r_{xy} - r_{yx})] \exp(-j2\theta) \\ r_{RR} = \frac{1}{2} [(r_{xx} - r_{yy}) + j(r_{xy} + r_{yx})] \exp(j2\theta) \\ r_{RL} = \frac{1}{2} [(r_{xx} + r_{yy}) + j(r_{xy} - r_{yx})] \\ r_{LR} = \frac{1}{2} [(r_{xx} + r_{yy}) - j(r_{xy} - r_{yx})] \end{cases}. \quad (3)$$

从(3)式中, 可以得出, $|r_{xx}| \approx |r_{yy}| \approx 1$, $|r_{xy}| \approx |r_{yx}| \approx 1$ 且两个交叉极化之间不存在相位差。此时, 可以得到反射系数的琼斯矩阵为

$$\mathbf{R} = \begin{bmatrix} 0 & 1 \\ 1 & 0 \end{bmatrix}. \quad (4)$$

反射波的极化与入射波的极化一致意味着在圆偏振波入射下, 相位是旋转角度的两倍。

为了拓宽单元结构的工作带宽, 所设计的单元结构的相位需要在不同频率处具有相似的斜率, 可表示为

$$\frac{\partial \varphi(L, L)}{\partial f_1} \approx \frac{\partial \varphi(L, L)}{\partial f_i} \approx \frac{\partial \varphi(L, L)}{\partial f_2}, \quad (5)$$

式中: f_1 、 f_2 表示工作频带中的低频和低频; f_i 表示频带内的任意频率; $\varphi(L, L)$ 表示左旋圆偏振波入射下的反射相位。右旋圆偏振波入射情况与左旋类似。为实现较宽的工作频带, 需要实现高频和低频的间隔较大。

2.2 单元结构设计

所设计的宽带、高效率单层双箭头反射单元结构, 如图 2 所示。该单元结构由三种结构构成, 分别为双箭头金属单元结构组成的超表面、聚酰亚胺介质层 (PI)、金属反射面。利用基于有限元法的 CST MICROWAVE STUDIO 电磁仿真软件对单元结构进行仿真, 设置端口条件为 Floquet, x 轴和 y 轴方向均

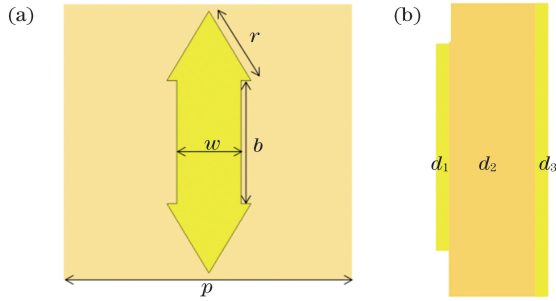
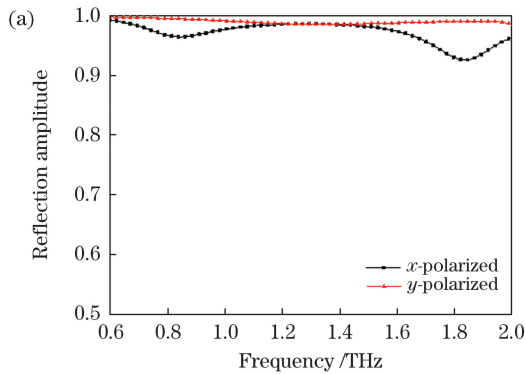


图 2 单层双箭头单元结构示意图。(a)顶视图；(b)侧视图
Fig. 2 Structural diagram of single-layer double-arrow unit. (a) Top view; (b) side view

采用 unit cell 周期性边界条件。优化所得参数为：电介质层周期 $p = 90 \mu\text{m}$ ，厚度 $d_2 = 35 \mu\text{m}$ ；顶部单层双



箭头的结构参数为 $r = 26 \mu\text{m}$, $b = 40 \mu\text{m}$, $w = 20 \mu\text{m}$ ，厚度 $d_1 = 0.2 \mu\text{m}$ ；底层金属厚度 $d_3 = 0.2 \mu\text{m}$ 。

入射波为沿 z 轴负方向垂直入射的太赫兹线偏振波，将频率范围设置为 $0.6 \sim 2.0 \text{ THz}$ 。不同频率下入射的 x 线偏振光和 y 线偏振光的反射振幅和反射相位如图 3(a)、(b) 所示。可以发现，在 $0.9 \sim 1.8 \text{ THz}$ 的宽带内，由于单元结构具有 45° 对称性，故入射的 x 线偏振光和 y 线偏振光的反射振幅均大于 0.9 且反射相位差接近 180° 。

当入射波为圆偏振波时，分析了顶部单层双箭头单元以其中心为原点， z 轴为旋转轴，旋转不同角度 θ 后的反射特性，如图 4 所示。从图 4(a)、(c) 中

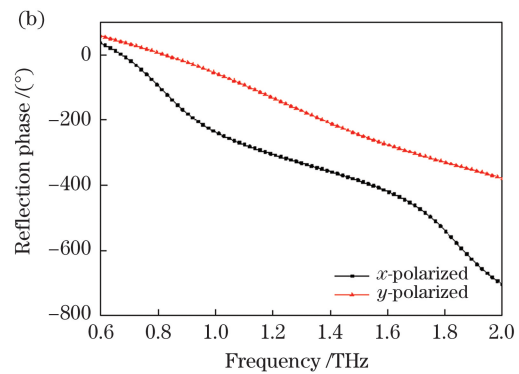


图 3 不同频率下的反射振幅和反射相位。(a)反射振幅；(b)反射相位

Fig. 3 Reflection amplitudes and reflection phases at different frequencies. (a) Reflection amplitudes; (b) reflection phases

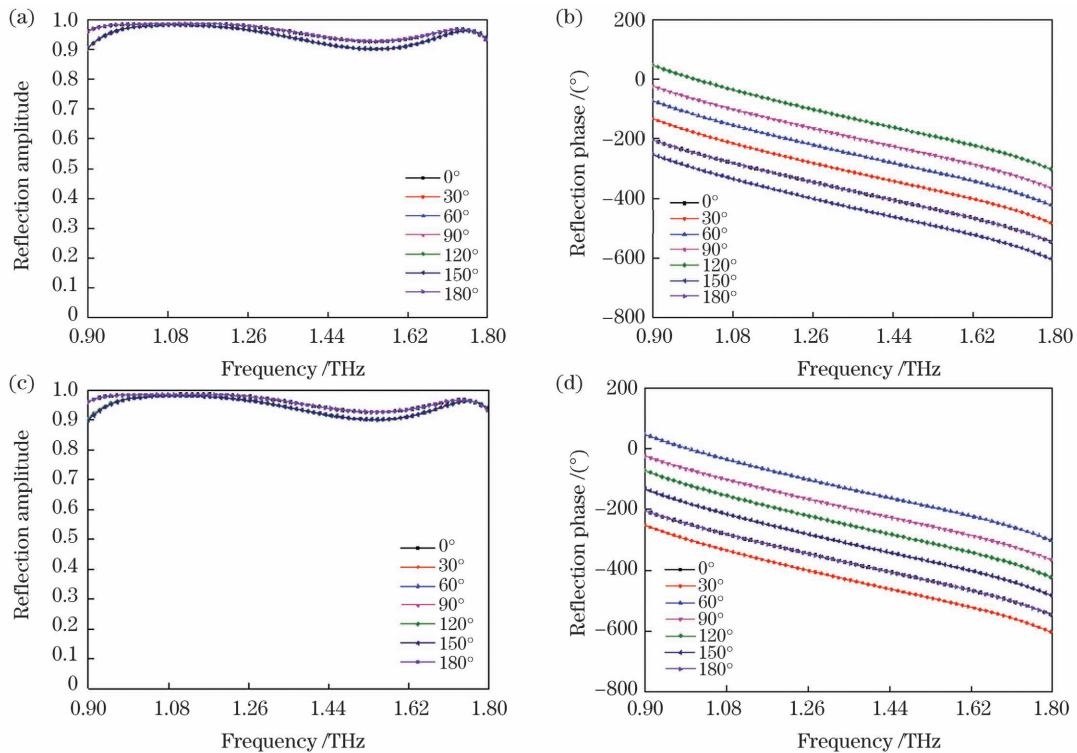


图 4 不同入射圆偏振光的反射振幅和反射相位。(a)(b)左旋圆偏振入射光；(c)(d)右旋圆偏振入射光

Fig. 4 Reflection amplitudes and reflection phases of different incident circular polarized light. (a) (b) Left-handed incident circular polarized light; (c) (d) right-handed incident circular polarized light

可以发现,在 0.9~1.8 THz 的宽带内,反射振幅均大于 0.9,且振幅变化相对稳定。从图 4(b)、(d)中可以发现,当左旋圆偏振光和右旋圆偏振光分别垂直入射所提结构时,在 0.9~1.8 THz 的宽带内,相位变化近似等于旋转角度的两倍。在 P-B 相位原理中,结构单元的旋转角度与反射偏振波的相位之间存在固定的数值关系,即后者为前者的两倍。上述结果与 P-B 相位原理一致。

3 反射式宽带超表面的设计与分析

对于所提的单层双箭头超表面,可以通过改变

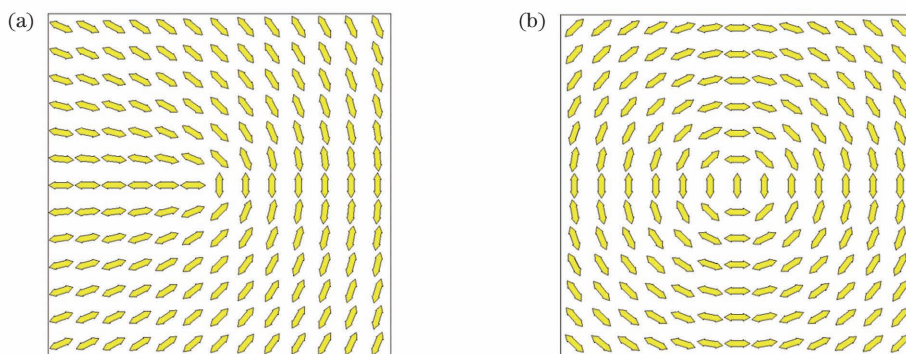


图 5 在不同拓扑荷数下,基于单层双箭头单元结构的反射式超表面。(a) $l=1$; (b) $l=2$

Fig. 5 Reflective metasurfaces based on single-layer double-arrow element structure at different topological charges.

(a) $l=1$; (b) $l=2$

频率 f 分别为 0.9、1.3、1.8 THz,距离超表面 500 μm (传播距离为 500 μm)下,涡旋波束的反射相位和反射振幅分布,如图 6 所示。可以看出,涡旋光束电场空间分布的主要特征为三个频率下的反射

相位分布来产生 OAM 涡旋光束,涡旋相位分布为

$$\varphi(x, y) = l \cdot \arctan\left(\frac{y}{x}\right). \quad (6)$$

3.1 涡旋光束的产生与宽带特性

图 5(a)、(b)分别为当 $l=1$ 和 $l=2$ 时,基于单层双箭头单元结构的 13×13 反射式超表面。利用 CST MICROWAVE STUDIO 进行全波仿真,工作频段设置为 0.8~2.0 THz,入射波沿 $-z$ 方向垂直入射到超表面。

观察涡旋波束在整个工作频段的产生情况以验证所设计反射超表面的宽带特性。给出了在工作

相位的的变化范围为 $0 \sim 2\pi$,呈现螺旋分布且沿逆时针方向旋转。图 6(b1)~(b3)中出现的中心暗环图案,证实了原点涡旋的存在,且波的奇点在整个传播过程中都是稳定的。

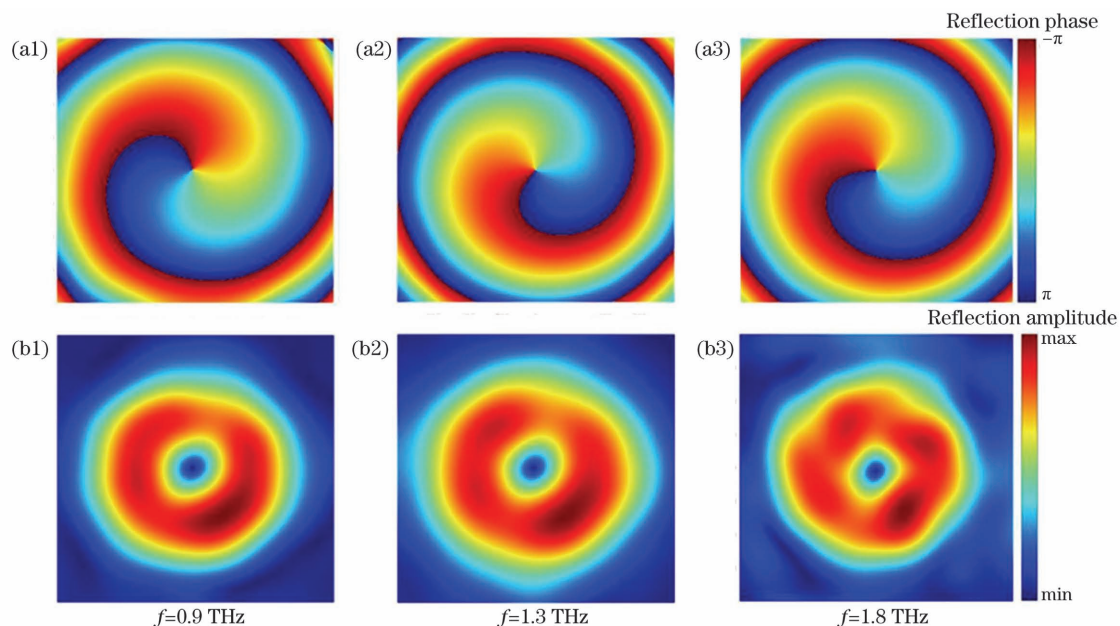


图 6 当 $l=1$ 时,不同频率下超表面产生的涡旋光束的反射相位和反射振幅

Fig. 6 Reflection phases and reflection amplitudes of vortex beams generated by metasurface at different frequencies when $l=1$

3.2 涡旋光束的传播特性

为了进一步观察不同传播距离下涡旋光束的传播特性,给出了工作频率 $f=0.9$ THz 时,传播距离

z_1 为 50、250、500、100 μm 下的涡旋光束的反射相位与反射振幅,如图 7 所示。可以看出,反射相位图逐渐螺旋化,反射振幅分布图逐渐趋于环形。

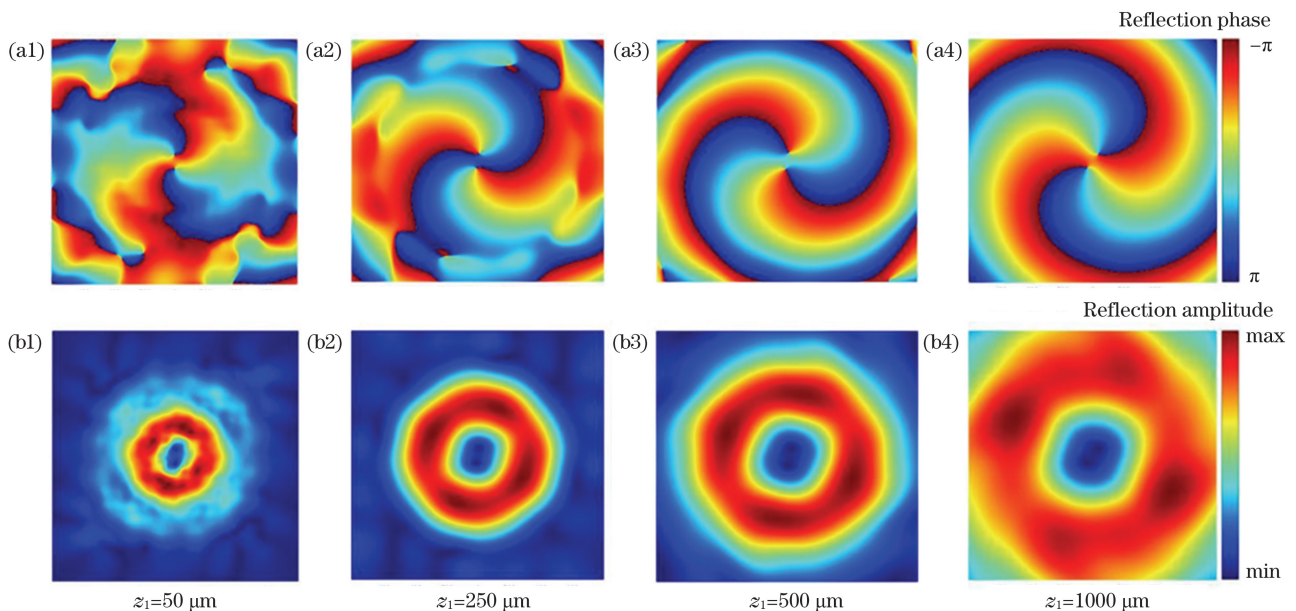


图 7 当 $l=2$ 时,不同传输距离下超表面产生的涡旋光束的反射相位和反射振幅

Fig. 7 Reflection phases and reflection amplitudes of vortex beams generated by metasurface at different transmission distances when $l=2$

4 结 论

设计了一种双箭头反射式宽带超表面。仿真结果表明,所设计的超表面结构可以在 $0.9\sim 1.8$ THz 频段内,圆偏振光正入射条件下,产生携带 OAM 的涡旋波束,并具有效率高、宽带、结构简单等优点。研究结果对利用超表面产生太赫兹涡旋波束有一定的参考价值。此外,所涉及的超表面结构简单、易实现、易集成,可以较容易地产生具有不同拓扑荷数的 OAM 波束,在太赫兹通信领域和 OAM 传输应用方面具有潜在的应用前景。

参 考 文 献

- [1] Beard M C, Turner G M, Schmuttenmaer C A. Terahertz spectroscopy[J]. The Journal of Physical Chemistry B, 2002, 106(29): 7146-7159.
- [2] Jepsen P U, Clark S J. Precise ab-initio prediction of terahertz vibrational modes in crystalline systems[J]. Chemical Physics Letters, 2007, 442(4/5/6): 275-280.
- [3] Hunsche S, Koch M, Brener I, et al. THz near-field imaging[J]. Optics Communications, 1998, 150(1/2/3/4/5/6): 22-26.
- [4] Meng F, Thomson M D, Blank V, et al. Characterizing large-area electro-optic crystals toward two-dimensional real-time terahertz imaging [J]. Applied Optics, 2009, 48(27): 5197-5204.
- [5] Köhler R, Tredicucci A, Beltram F, et al. Terahertz semiconductor-heterostructure lasers [J]. Nature, 2002, 417: 156-159.
- [6] Li T J, Sun Y, Shao G F, et al. Terahertz nondestructive detection method of ceramic matrix composites[J]. Laser & Optoelectronics Progress, 2018, 55(6): 061101. 李铁军, 孙跃, 邵桂芳, 等. 陶瓷基复合材料的太赫兹无损检测方法[J]. 激光与光电子学进展, 2018, 55(6): 061101.
- [7] Wang J, Yang J Y, Fazal I M, et al. Terabit free-space data transmission employing orbital angular momentum multiplexing [J]. Nature Photonics, 2012, 6(7): 488-496.
- [8] Wang W, Guo Z Y, Sun Y X, et al. Ultra-thin optical vortex phase plate based on the L-shaped nanoantenna for both linear and circular polarized incidences[J]. Optics Communications, 2015, 355: 321-325.
- [9] Allen L, Beijersbergen M W, Spreeuw R J C, et al. Orbital angular momentum of light and the transformation of Laguerre-Gaussian laser modes[J]. Physical Review A, 1992, 45(11): 8185-8189.
- [10] Padgett M, Courtial J, Allen L. Light's orbital

- angular momentum [J]. *Physics Today*, 2004, 57 (5): 35-40.
- [11] Yao A M, Padgett M J. Orbital angular momentum: origins, behavior and applications [J]. *Advances in Optics and Photonics*, 2011, 3(2): 161-204.
- [12] Zeng J, Chen Y H, Liu X L, et al. Research progress on partially coherent vortex beams [J]. *Acta Optica Sinica*, 2019, 39(1): 0126004.
曾军, 陈亚红, 刘显龙, 等. 部分相干涡旋光束研究进展 [J]. *光学学报*, 2019, 39(1): 0126004.
- [13] Luo M. Design of hook-typed metasurface for vortex beams generation [J]. *Laser & Optoelectronics Progress*, 2021, 58(1): 0108001.
罗蒙. 一种产生涡旋光束的勾型阵列超表面结构设计 [J]. *激光与光电子学进展*, 2021, 58 (1): 0108001.
- [14] Uchida M, Tonomura A. Generation of electron beams carrying orbital angular momentum [J]. *Nature*, 2010, 464(7289): 737-739.
- [15] Ostrovsky A S, Rickenstorff-Parrao C, Arrizón Victor. Generation of the “perfect” optical vortex using a liquid-crystal spatial light modulator [J]. *Optics Letters*, 2013, 38(4): 534-536.
- [16] Wang H C, Hu A J, Chen P F. Generation of Laguerre-Gaussian beam based on spatial light modulator [J]. *Laser Technology*, 2017, 41(3): 447-450.
汪慧超, 胡阿健, 陈培锋. 空间光调制器产生拉盖尔-高斯光束方法研究 [J]. *激光技术*, 2017, 41(3): 447-450.
- [17] Mirhosseini M, Magaña-Loaiza O S, Chen C C, et al. Rapid generation of light beams carrying orbital angular momentum [J]. *Optics Express*, 2013, 21 (25): 30196-30203.
- [18] Sheng C, Liu H, Zhu S N. Research process of transformation optics based on metasurface [J]. *Laser & Optoelectronics Progress*, 2019, 56(20): 202402.
盛冲, 刘辉, 祝世宁. 超表面变换光学研究进展 [J]. *激光与光电子学进展*, 2019, 56(20): 202402.
- [19] Yu N F, Genevet P, Kats M A, et al. Light propagation with phase discontinuities: generalized laws of reflection and refraction [J]. *Science*, 2011, 334(6054): 333-337.
- [20] He J W, Wang X K, Hu D, et al. Generation and evolution of the terahertz vortex beam [J]. *Optics Express*, 2013, 21(17): 20230-20239.
- [21] Yu S X, Li L, Shi G M. Dual-polarization and dual-mode orbital angular momentum radio vortex beam generated by using reflective metasurface [J]. *Applied Physics Express*, 2016, 9(8): 082202.
- [22] Xu H X, Liu H W, Ling X H, et al. Broadband vortex beam generation using multimode Pancharatnam-Berry metasurface [J]. *IEEE Transactions on Antennas and Propagation*, 2017, 65 (12): 7378-7382.
- [23] Gibson G, Courtial J, Padgett M J, et al. Free-space information transfer using light beams carrying orbital angular momentum [J]. *Optics Express*, 2004, 12(22): 5448-5456.
- [24] Xu H X, Wang G M, Cai T, et al. Tunable Pancharatnam-Berry metasurface for dynamical and high-efficiency anomalous reflection [J]. *Optics Express*, 2016, 24(24): 27836-27848.

Generation of Broadband Terahertz Vortex Beam Based on Double-Arrow Metasurface

Guo jiaoyan^{1,2,3}, Li Wenyu^{1,2,3}, Sun Ran^{1,2,3}, Zhao Guozhong^{1,2,3*}

¹ Department of Physics, Capital Normal University, Beijing 100048, China;

² Beijing Advanced Innovation Center for Imaging Theory and Technology, Beijing 100048, China;

³ Key Laboratory of Terahertz Optoelectronics, Ministry of Education, Capital Normal University, Beijing 100048, China

Abstract

Objective An electromagnetic wave with a spiral wavefront is a vortex beam with an orbital angular momentum (OAM). The OAM vortex beam has a phase factor $\exp(il\varphi)$, φ is the azimuth angle, and l is the topological charge (integer or non-integer). The vortex beam's wavefront propagates in a spiral forward, and the intensity of the beam center is close to zero. This unique electromagnetic characteristic has potential applications in optics, atomic physics, and communications. In recent years, the massive capability potential has benefited humans, and the broadband characteristics are the key to effectively improving the channel capacity. Most of the current vortex beam generating devices have shortcomings such as narrow bandwidth and low working efficiency. Methods like spiral

phase plates and spatial light modulators are employed in previous studies to generate vortex beams. These methods produce optical devices with issues such as large size and high price. Because metasurfaces can control the phase, amplitude, and polarization of electromagnetic wavefronts, using metasurfaces to generate vortex beams has become a novel method. This method is simple in structure and low in loss, making it ideal for integration development.

Methods This paper proposes a terahertz broadband vortex beam generator based on the metasurface of a single-layer double-arrow unit structure. The device is composed of a three-layer metasurface-dielectric-metal structure. The top layer is a metasurface consisting of double-arrow metal structural units, the middle layer is a polyimide, and the bottom metal layer is gold. CST MICROWAVE STUDIO is employed to simulate the reflection performance of the unit structure. Better performance is obtained after optimizing the structural parameters, and a set of optimized structural parameters is determined (Fig. 2). The reflection characteristics of the top single-layer double-arrow unit with its center as the origin and the z -axis as the rotation axis are analyzed when the incident light is set as a circularly polarized wave. Reflective broadband metasurfaces with various topological charges are designed using the unit structure's ordered arrangement to generate the corresponding vortex beams based on the Pancharatnam-Berry (P-B) phase principle. Metasurfaces with topological charges of 1 and 2 are designed in this study. CST MICROWAVE STUDIO software simulates the reflection amplitudes and phases of the circularly polarized terahertz beams perpendicular to the metasurface and verifies the designed reflective metasurface's broadband and propagation characteristics.

Results and Discussions When the incident wave is circularly polarized, the center of the metal structure of the top double-arrow unit is set as the origin, and the z -axis is the rotation axis. The reflection amplitude change is relatively stable in the broadband range of 0.9–1.8 THz under different rotation angles, and the phase change with angle is approximately equal to twice the rotation angle (Fig. 4). The broadband and propagation characteristics of the designed reflective metasurface are verified to observe the generation of vortex beams in the entire operating frequency band. The operating frequency of a circularly polarized wave incident perpendicular to a metasurface with a topological charge of 1 is $f = 0.9, 1.3, 1.8$ THz, and the vortex beam's reflection phases and amplitudes at a distance of 500 μm from the metasurface is given (Fig. 6). It reveals that the reflection phases at the three frequencies are continuously distributed at $0-2\pi$, with a spiral distribution and rotating in a counterclockwise direction. The central dark ring pattern of the near field can be seen in Fig. 6, confirming the existence of the origin vortex and the wave's singularity in the whole beam. When the working frequency of the metasurface with a topological charge of 2 is $f = 0.9$ THz, the vortex beam's reflection phases and amplitudes at the propagation distance of 50, 250, 500, and 1000 μm are given (Fig. 7), and the phase diagrams gradually spiral, while the amplitude distribution diagrams gradually tend to a ring, indicating that the vortex beam has better propagation characteristics in the operating frequency range.

Conclusions The simulation results show that the designed unit structure can achieve reflection amplitudes with over 90% efficiency through various rotation angles. The metasurface is designed in the frequency range of 0.90–1.80 THz, which can effectively convert circular polarized terahertz beams into vortex beams with OAM with different topological charges. It has the advantages of high efficiency, broadband, and simple structure and has a particular reference value for using metasurfaces to generate terahertz vortex beams.

Key words optical communications; terahertz; vortex beam; broadband; metasurface

OCIS codes 060.4080; 050.4865